Electronic Supplementary Material (ESI) for ChemComm.

Amorphous FeNi-bimetallic Infinite Coordination Polymers as Advanced Electrocatalysts for the Oxygen Evolution Reaction

Junchao Ma,[a] Xiaojue Bai,[a] Wenxiu He,[a] Sha Wang,[a] Linlin Li,[a] Huan Chen,[a] Tieqiang Wang,[a] Xuemin Zhang,[a] Yunong Li,[a] Liying Zhang,[a] Junyi Chen,[b] Fanbao Meng*[a] and Yu Fu*[a]

[a] Department of Chemistry, College of Sciences, Northeastern University, Shenyang 110819, P. R. China.

[b] Engineering Laboratory of Chemical Resources Utilization in South Xinjiang of Xinjiang Production and Construction Corps, College of Life Science, Tarim University, Xinjiang Uygur Autonomous Region, Alaer, 843300, P. R. China.

Corresponding Author

* E-mail: fuyu@mail.neu.edu.cn (Yu Fu)

* E-mail: mengfb@mail.neu.edu.cn (Fanbao Meng)

Experimental Section

Materials

All chemicals used in this work were analytical grade and without further purification. 2-aminoterephthalic acid ($H_2BDC\text{-}NH_2$), 1,4-benzenedicarboxylate (H_2BDC), 1,4-naphthalenedicarboxylic acid (H_2(1,4-NDC)), 2,6-naphthalenedicarboxylic acid (H_2(2,6-NDC)), 2,5-dihydroxyterephthalic acid (H_2DOBDC), trimedic acid (H_3BTC) were purchased from Energy Chemical. Iron chloride tetrahydrate ($FeCl_2 \cdot 4H_2O$) were purchased form Tianjin bailunsi biotechnology Co. Ltd. Nickel (II) acetate tetrahydrate [$(CH_3COO)_2Ni \cdot 4H_2O$], ethanol ($C_2H_5OH$), acetonitrile ($CH_3CN$) and N,N-dimethylformamide (DMF) were purchased from Sinopharm Chemical Reagent Co. Ltd.

Synthesis of bimetallic $Fe_xNi_y(BDC\text{-}NH_2)$ ICPs

Take the synthesis of $Fe_1Ni_2(BDC\text{-}NH_2)$ ICP as a typical example. 0.09 mmol of $FeCl_2 \cdot 4H_2O$ (17.9 mg) and 0.18 mmol of $(CH_3COO)_2Ni \cdot 4H_2O$ (44.8 mg) were dissolved in a 30 mL mixture of DMF and CH_3CN (V:V=1:2) as the metal precursor solution. The organic ligand solution was dissolving 0.39 mmol of $H_2BDC\text{-}NH_2$ (70.6 mg) into the mixture of 20 ml of DMF and 10 ml of CH_3CN. Then the metal precursor solution was directly added into linker solution under magnetic stirring 1 h at room temperature. As time goes by, the deep yellow precipitation was gradually increasing. Finally, the product was centrifuged and washed with DMF three times to obtain $Fe_1Ni_2(BDC\text{-}NH_2)$ ICP. The synthesis of the $Fe_xNi_y(BDC\text{-}NH_2)$ ICPs with diverse metallic ratios only need to adjust the ions concentrations of $FeCl_2 \cdot 4H_2O$ and

$(CH_3COO)_2Ni \cdot 4H_2O$. At the same time, the preparation method and all ions concentrations of other FeNi-bimetallic ICPs with different ligands were consistent with the above method.

Preparation of catalytic electrodes

The products were uniformly dispersed into 5 ml ethanol. Ni foam substrates were impregnated directly into the teflon cap of containing 2.2 ml samples. Then put them in the air and make the solvent volatilize completely at the room temperature.

Characterization

The morphology of Fe_1Ni_2(BDC-NH_2) ICP was characterized with a field emission scanning electron microscope (FE-SEM, Hitachi SU8010) and corresponding elemental mapping images were captured on energy-dispersive X-ray (EDX, Oxford Instruments). The crystal structure of the product was tested by X-ray diffraction (XRD) on PANalytical Empyrean X-ray diffractometer in the 2θ range of 5−40° with Cu Kα1 (λ = 1.5406 Å) radiation. The X-ray photoelectron spectroscopy (XPS) measurements were carried out on Thermo Scientific ESCALAB 250 apparatus to affirm elemental valence states of the electrocatalyst. The organic groups and specific surface areas/pore sizes of the samples were characterized by fourier transform infrared spectroscopy (FT-IR, Bruker VERTEX 70) and nitrogen adsorption-desorption isotherms at 77 K (Micromeritics ASAP 2020 system). The actual ratio of Fe and Ni content in the Fe_1Ni_2(BDC-NH_2) was measured by the inductively coupled plasma-optical emission spectroscopy (ICP-OES) on a PerkinElmer Optima 2100DV ICP-OES spectrometer.

ICP-OES measurement

The sample of Fe_1Ni_2(BDC-NH_2), where the feeding ratio of Fe to Ni is 1:2, was measured by ICP-OES, indicating the mole ratio of Fe to Ni in the sample is 1:2.45.

Electrochemical Test

The electrochemical performance of catalytic electrodes was measured by electrochemical workstation (CHI660E, Shanghai Chenhua Instrument Co., Ltd.)). The liner sweep voltammetry (LSV) was performed by sweeping the potential from 1.0 V to 1.8 V at a scan rate of 5 mV • s^{-1}. Electrochemical impedance spectroscopy (EIS) was carried out at the polarization potential 1.53 V. The electrochemical double layer capacitance (C_{dl}) was obtained by cyclic voltammetry (CV) in a region of non-Faradaic (0.2 V-0.3 V vs. Ag/AgCl) at different scan rates of 20, 40, 60, 80, 100, 120 mV • s^{-1}, respectively. The stability tests were proceeded from chronoamperometry (j-t) at a constant voltage of 0.49 V vs.Ag/AgCl for 12 hours and the comparison of LSV curves after 1000 CV cycles at a sweep rate of 20 mV • s^{-1} .

RHE calibration

We used the Ag/AgCl electrode as the reference electrode in all measurements. The potentials reported here were calibrated with respect to the reversible hydrogen electrode (RHE). The calibration was performed in H_2-saturated 1.0 mol/L KOH and Pt sheets were used as working and counter electrodes. CV curve was measured at scan rate of 1 mV·s^{-1} and the average of two potentials at 0 mA current was taken to be the thermodynamic potential for the hydrogen electrode reactions.

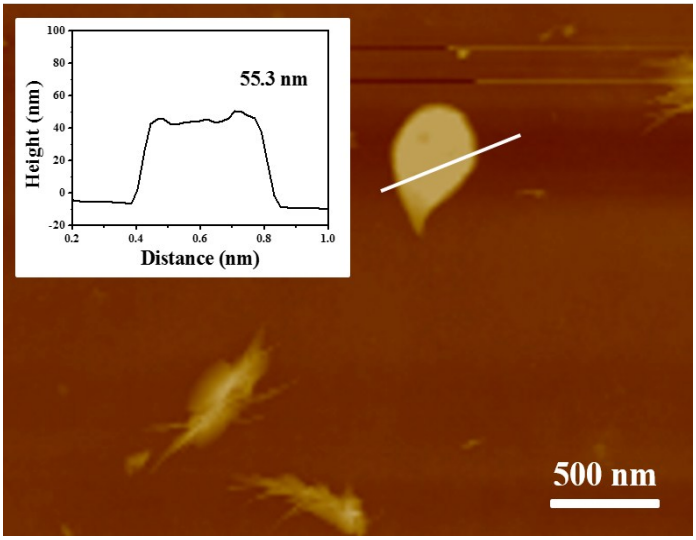

Fig. S1 AFM image of as-prepared Fe_1Ni_2(BDC-NH_2) ICP nanosheets.

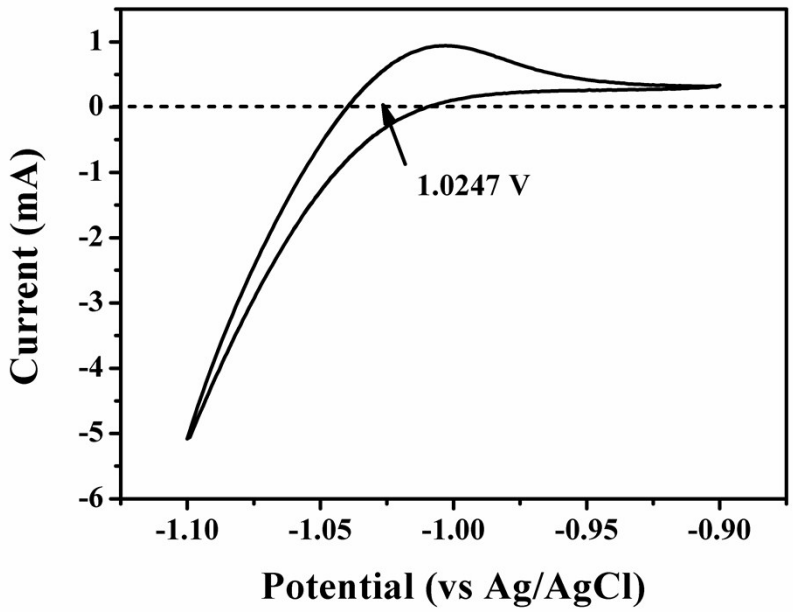

Fig. S2 CV curve of hydrogen electrode reaction.

So the 1 M KOH, E (RHE) = E (Ag/AgCl) + 1.0247V.

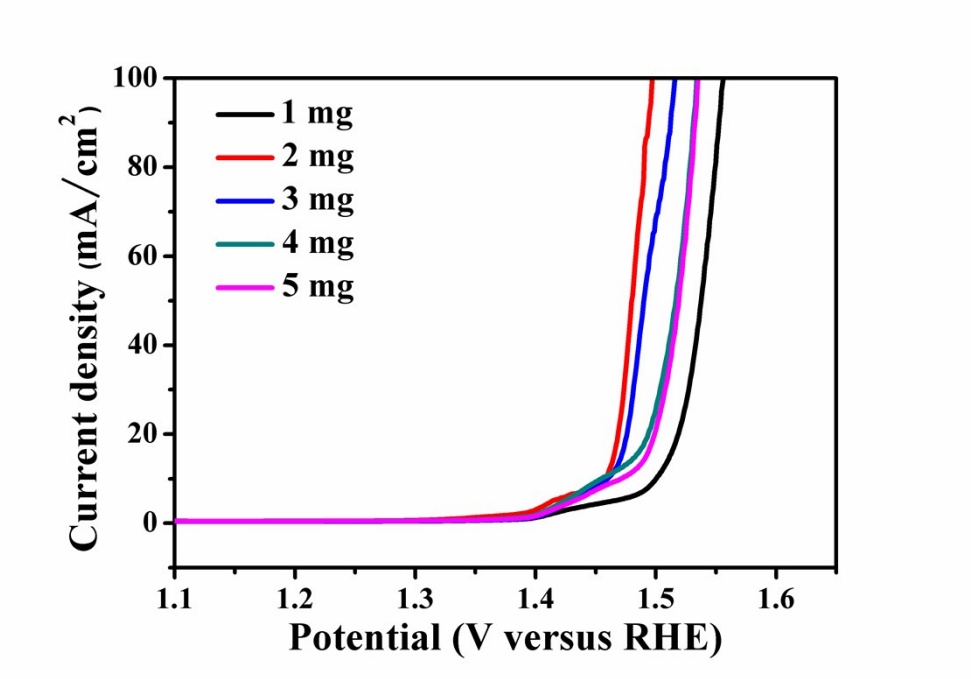

Fig. S3 LSV curves of Fe_1Ni_2(BDC-NH_2)/NF with different loading amounts.

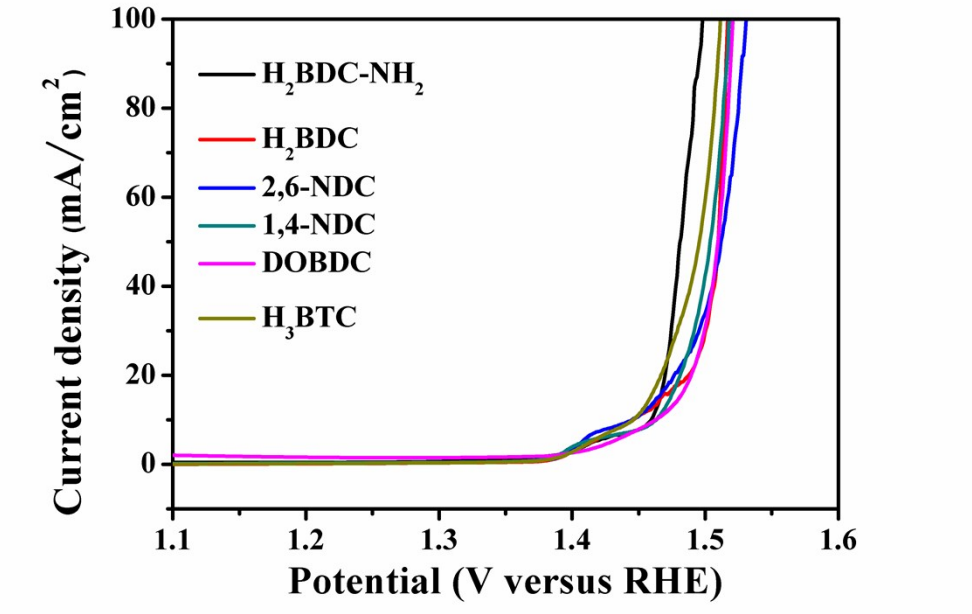

Fig. S4 LSV curves of Fe_1Ni_2 bimetallic ICPs/NF electrodes with different ligands.

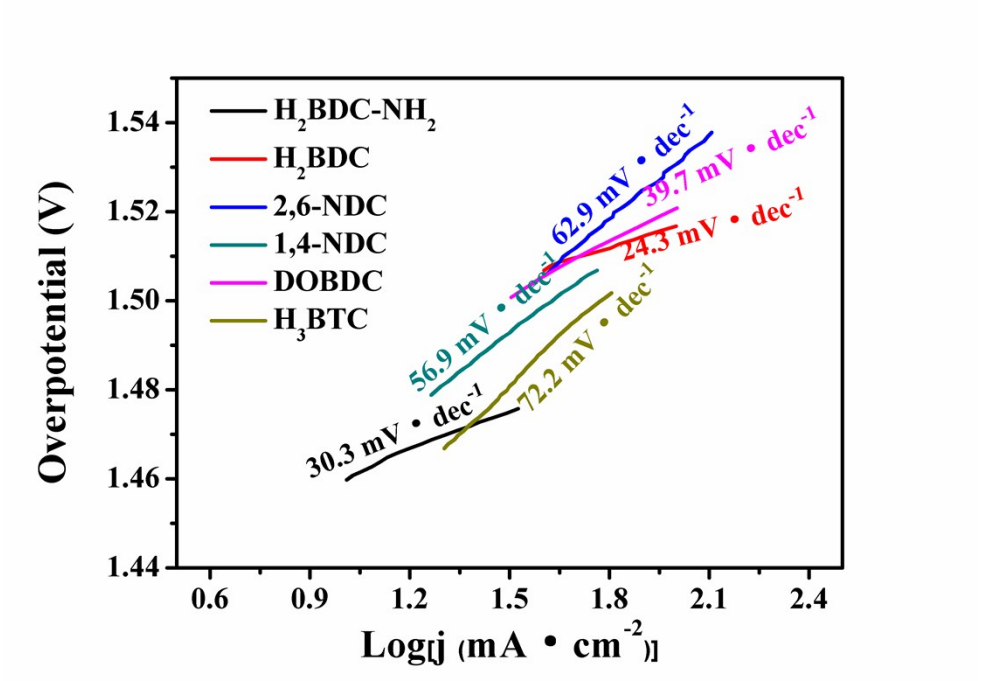

Fig. S5 Tafel plots of Fe_1Ni_2 bimetallic ICP/NF electrodes with different ligands.

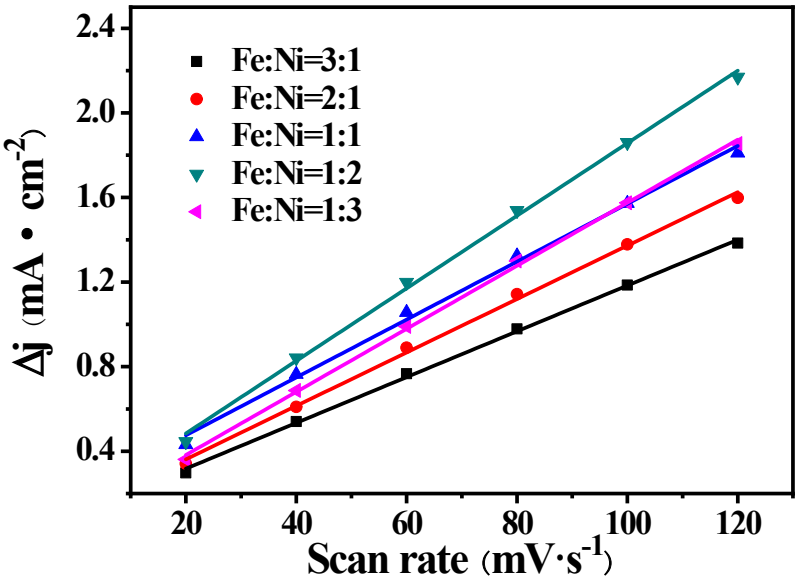

Fig. S6 The C_{dl} of $Fe_xNi_y(BDC\text{-}NH_2)$/NF with different ratios of Fe and Ni.

The C_{dl} value of the $Fe_xNi_y(BDC\text{-}NH_2)$/NF with 1:2 ratio is confirmed to be 17.16 $mF \cdot cm^{-2}$, which is higher than the other electrodes with ratios of 3:1 (10.83 $mF \cdot cm^{-2}$),

2:1 (12.63 $mF \cdot cm^{-2}$), 1:1 (13.69 $mF \cdot cm^{-2}$) and 1:3 (14.91 $mF \cdot cm^{-2}$).

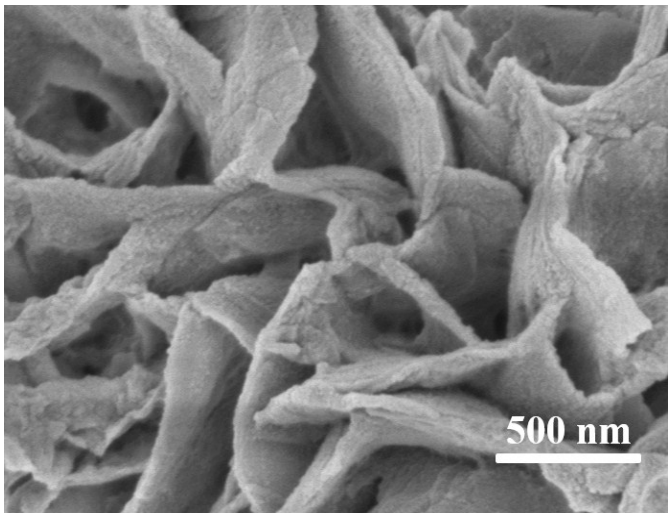

Fig. S7 SEM image of Fe_1Ni_2(BDC-NH_2)/NF after stability measurement of OER.

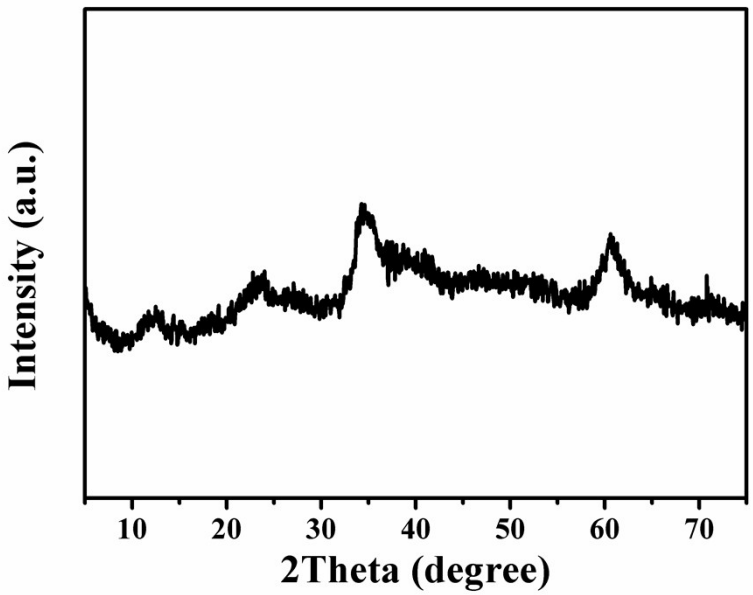

Fig. S8 XRD pattern of Fe_1Ni_2(BDC-NH_2) ICP after stability measurement of OER.

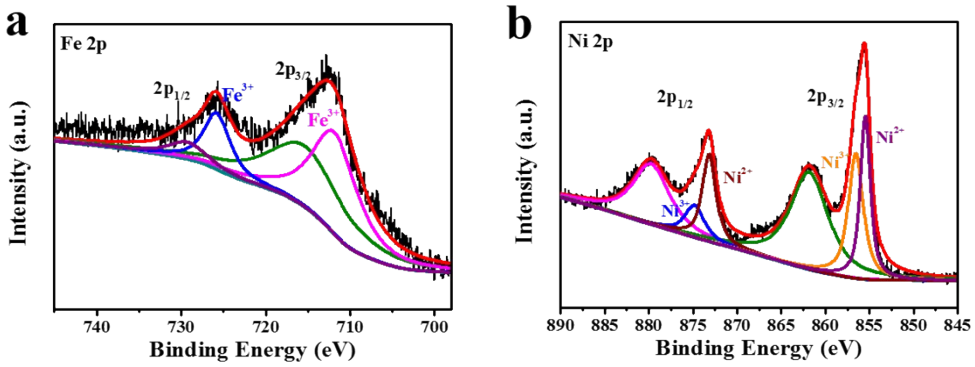

Fig. S9 High-resolution XPS spectras of (a) Fe 2p and (b) Ni 2p of Fe_1Ni_2(BDC-NH_2) ICP after stability measurement of OER.

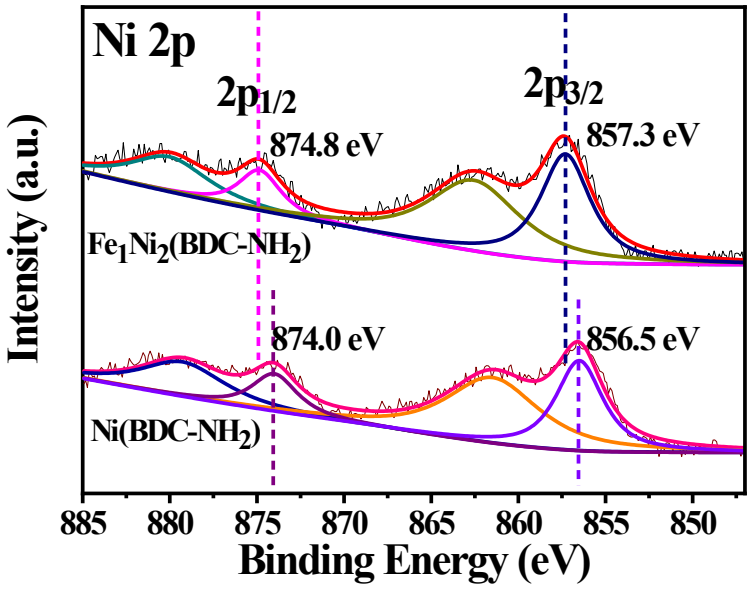

Fig. S10 High-resolution Ni 2p XPS spectra of Ni(BDC-NH_2) and Fe_1Ni_2(BDC-NH_2).

Table S1 The OER catalytic performances comparison of the recently reported catalysts.

Catalyst	Overpotential (mV)	Tafel slope (mV dec^{-1})	Electrolyte	Reference
Fe_1Ni_2(BDC-NH_2)	228 @ 10 mA·cm^{-2}	30.3	1 M KOH	This work
$CoSe_2$@DG composite	270 @ 10 mA·cm^{-2}	64	0.1 M KOH	1
o-$CoSe_2$-O UNs	251 @ 10 mA·cm^{-2}	73	1 M KOH	2
MIL-53(FeNi)/NF	233 @ 50 mA·cm^{-2}	31.3	1 M KOH	3
FeNi-O nanosheets	213 @ 10 mA·cm^{-2}	32	1 M KOH	4
$FeNi_{4.34}$@FeNi-foil	283 @ 10 mA·cm^{-2}	53	1 M KOH	5
Ni-MOF@Fe-MOF	265 @ 10 mA·cm^{-2}	82	1 M KOH	6
Fe_1Co_3/V_O-800	260 @ 10 mA·cm^{-2}	53	1 M KOH	7
MIL-100(FeNi)/NF	243 @ 10 mA·cm^{-2}	30.4	1 M KOH	8
NiFe-MOF-74	223 @ 10 mA·cm^{-2}	71.6	1 M KOH	9
NiFe-MOF	240 @ 10 mA·cm^{-2}	34	0.1 M KOH	10

References:

1. X. Wang, L. Zhuang, T. He, Y. Jia, L. Zhang, X. Yan, M. Gao, A. Du, Z. Zhu, X. Yao and S. H. Yu, *iScience*, 2018, **7**, 145-153.
2. X. Wang, L. Z. Zhuang, Y. Jia, H. L. Liu, X. C. Yan, L. Z. Zhang, D. J. Yang, Z. H. Zhu and X. D. Yao, *Angew. Chem. Int. Ed.*, 2018, **57**, 16421-16425.
3. F. Z. Sun, G. Wang, Y. Q. Ding, C. Wang, B. B. Yuan and Y. Q. Lin, *Adv. Energy Mater.*, 2018, **8**, 11.
4. X. Long, Z. J. Ma, H. Yu, X. Y. Gao, X. Y. Pan, X. X. Chen, S. H. Yang and Z. G. Yi, *J. Mater. Chem. A*, 2016, **4**, 14939-14943.
5. U. Y. Qazi, C. Z. Yuan, N. Ullah, Y. F. Jiang, M. Imran, A. Zeb, S. J. Zhao, R. Javaid and A. W. Xu, *ACS Appl. Mater. Interfaces*, 2017, **9**, 28627-28634.
6. K. Rui, G. Zhao, Y. Chen, Y. Lin, Q. Zhou, J. Chen, J. Zhu, W. Sun, W. Huang and S. X. Dou, *Adv. Funct. Mater.*, 2018, **28**, 1801554.
7. W. X. Chen, Y. W. Zhang, G. L. Chen, R. Huang, Y. M. Zhou, Y. J. Wu, Y. J. Hu and K. Ostrikov, *J. Mater. Chem. A*, 2019, **7**, 3090-3100.
8. C. Q. Li, Y. W. Liu, G. Wang, L. H. Guan and Y. Q. Lin, *ACS Sustainable Chem. Eng.*, 2019, **7**, 7496-7501.
9. J. L. Xing, K. L. Guo, Z. H. Zou, M. M. Cai, J. Du and C. L. Xu, *Chem. Commun.*, 2018, **54**, 7046-7049.
10. J. Duan, S. Chen and C. Zhao, *Nat Commun*, 2017, **8**, 15341.